Synthesis of Sinusoidal Waveform References Synchronized With Periodic Signals

Claudio Alberto Busada, Héctor Gerardo Chiacchiarini, *Senior Member, IEEE*, and Juan Carlos Balda, *Senior Member, IEEE*

***Abstract*—This paper proposes a novel method to generate a sinusoidal waveform synchronized with any measurable periodic signal whose frequency is within a given neighborhood. The synthesized sinusoidal signal could be used as a reference current for certain applications of parallel active power filters or any other where such synchronization would be necessary (e.g., ac/dc converters for renewable energy resources, power factor correctors, power supplies, UPS, etc.) The method is based on the behavior of a dynamical system and avoids employing the usual combination of phase-locked loop (PLL) and lookup table found in most parallel active filters synthesizing a sinusoidal source current (a table also means using significant storage memory). The novel method produces two high-quality sinusoidal waveforms that are in quadrature and is applicable to those parallel active filters whose control methodology is in the $\alpha\beta$ reference frame, or alternatively, it produces three sinusoidal waveforms shifted 120 degrees for designs that work in the abc frame. Here, a $(2n+1)$th order implementation is described, including a proof of convergence. For its most simple implementation $(n = 1)$, simulated and experimental results are included.**

I. Introduction

THE use of parallel active power filters is one strategy to compensate for undesired current components in distribution lines. The filter could be thought as a controlled current source that injects in the distribution line, in parallel with the load, the opposite of the undesired load current components. Some active filter control strategies synthesize a sinusoidal reference source current [1], in contraposition to those control strategies that synthesize a resistive load behavior [2]. Similar needs appear in other applications such as ac/dc converters for renewable energy resources, power factor correctors, power supplies, UPS, etc. The sinusoidal reference source currents can be computed in the $\alpha\beta$ reference frame [3], [4], [5], [6] or in the abc frame [7], [8]. In the first case, two quadrature sinusoidal waveforms are needed, and in the second case, they must be shifted by 120 degrees. A phase-locked loop (PLL) running at a frequency that is an integer multiple of the line frequency (e.g., 1024 times) is a common method to generate these sinusoidal waveforms [6]. The PLL signal is used to increment a counter addressing a look-up table containing the sine function. Some events, such as the zero crossing point of the phase voltage, synchronize the reading of the zero of the sine function. Other approaches use three PLL-based voltage-controlled oscillators (VCO) to produce the desired sinusoidal signals [9]. Other authors [10] proposed a decoupled double synchronous reference frame PLL for detection of the positive sequence of three-phase power systems.

This paper proposes a novel method to generate these sinusoidal signals used as reference in parallel active power filters and other applications. The method avoids the use of the additional control hardware or software look up tables required by conventional methods, and the waveform synthesis is obtained from the output of a dynamical system, which provides the required sinusoidal signals. This dynamical system in its basic version has only three states so a relatively low computational burden is added to the system controller in a digital implementation. The output has good quality for most practical applications. Simulation and experimental results are given to illustrate the feasibility of the proposed ideas. This work expands the results shown in [11], including here a higher order realization of the algorithm, and a convergence proof of the adaptive algorithm.

This work is organized as follows: Section II describes the proposed dynamical system. Section III analyzes the system by including a stability proof. Section IV describes the discrete implementation of the system being useful for real-time operation. Section V shows selected simulations and experimental results illustrating the quality of the obtained sinusoidal waveforms. Finally Section VI presents the conclusions.

II. The Proposed Dynamical System

This section describes the proposed dynamical system used for generating two (or three) sinusoidal waveforms, phase shifted adequately and useful for control purposes in active filtering applications (or any other application having similar requirements). The dynamical system synthesizes the sinusoidal signal using a measured input waveform as reference (e.g., the load current i_L, or the line voltage, v_s, in the case of single-phase systems). A two-dimensional output vector (called $\vec{i}_{sf}^{\,\alpha\beta}$ or $\vec{v}_{sf}^{\,\alpha\beta}$, respectively) is generated, containing information about the phase and amplitude of the component at the fundamental frequency of the original measured waveform.

To present the proposed idea, consider that the line voltage v_s is a stationary input waveform (although slow variations will be later allowed). The output vector will be $\vec{v}_{sf}^{\,\alpha\beta} = [v_{sf\alpha}\ \ v_{sf\beta}]^T$

Manuscript received June 5, 2007; revised September 28, 2007. This work supported in part by Universidad Nacional del Sur (under research Grants PGI UNS 24/K021 and 24/K033), the Agencia Nacional de Promocion Científica y Tecnológica (under research Grant PICT'98 3963, PICTO-UNS 814, and PICT04 21811) and CONICET (PIP04 6101). This paper was previously presented in part at the 35th IEEE Power Electronics Specialists Conference 2004 (PESC04), Aachen, Germany, June 20-25, 2004, as "Sinusoidal waveform synthesis for parallel active filter applications".T Recommended for publication by Associate Editor V. Staudt.

C. A. Busada and H. G. Chiacchiarini are with the Instituto de Investigaciones en Ingeniería Eléctrica "Alfredo C. Desages" (UNS-CONICET), Departamento de Ingeniería Eléctrica y Computadoras, Universidad Nacional del Sur, Bahía Blanca, Argentina (e-mail: cbusada@criba.edu.ar; hgch@ieee.org).

J. C. Balda is with the Department of Electrical Engineering, University of Arkansas, Fayetteville, AR 72701 USA (e-mail: jbalda@uark.edu).

Digital Object Identifier 10.1109/TPEL.2007.915777

where $v_{sf\alpha}$ is the fundamental frequency component of v_s scaled in amplitude (practically without errors in phase and frequency). The $v_{sf\beta}$ component is a waveform 90° shifted with respect to $v_{sf\alpha}$. The main characteristics of the output vector will remain in steady state, despite the existence of slow and bounded line frequency variations.

The general equations describing the dynamical system are

$$\begin{aligned}
\dot{\vec{x}}_1^{\alpha\beta} &= \vec{x}_2^{\alpha\beta} + \bar{\omega}\, P\, \vec{x}_1^{\alpha\beta} \\
\dot{\vec{x}}_2^{\alpha\beta} &= \vec{x}_3^{\alpha\beta} + \bar{\omega}\, P\, \vec{x}_2^{\alpha\beta} \\
&\vdots \\
\dot{\vec{x}}_{n-1}^{\alpha\beta} &= \vec{x}_n^{\alpha\beta} + \bar{\omega}\, P\, \vec{x}_{n-1}^{\alpha\beta}; \\
\dot{\vec{x}}_n^{\alpha\beta} &= -a_1 \vec{x}_1^{\alpha\beta} - \cdots - a_n \vec{x}_n^{\alpha\beta} + \bar{\omega}\, P\, \vec{x}_n^{\alpha\beta} + \vec{v}_s^{\alpha\beta} \\
\vec{v}_{sf}^{\alpha\beta} &= c_1 \vec{x}_1^{\alpha\beta} + \cdots + c_n \vec{x}_n^{\alpha\beta} \qquad (1)
\end{aligned}$$

$$\dot{\hat{\omega}} = \frac{1}{\tau}\left(-\hat{\omega} + \frac{v_{sf\alpha}\dot{v}_{sf\beta} - v_{sf\beta}\dot{v}_{sf\alpha}}{\left|\vec{v}_{sf}^{\alpha\beta}\right|^2}\right) \qquad (2)$$

$$\bar{\omega} = \mathrm{sat}(\hat{\omega}) \qquad (3)$$

where $\mathrm{sat}(\hat{\omega})$ is a saturation function given by

$$\mathrm{sat}(\hat{\omega}) = \begin{cases} \omega_{\max} & \text{if } \hat{\omega} > \omega_{\max} \\ \hat{\omega} & \text{if } \omega_{\min} \leqslant \hat{\omega} \leqslant \omega_{\max} \\ \omega_{\min} & \text{if } \hat{\omega} < \omega_{\min} \end{cases} \qquad (4)$$

and $0 < \omega_{\min} \leqslant \omega_{\max}$ define the neighborhood where the actual angular frequency $\omega = 2\pi f$ belongs (being f the actual line frequency in Hertz). Also

$$P = \begin{bmatrix} 0 & -1 \\ 1 & 0 \end{bmatrix}$$

is a rotation matrix, n is a design parameter, $2n+1$ is the order of the system, $\vec{x}_j^{\alpha\beta} = [x_{j\alpha}\ x_{j\beta}]^T, 1 \leqslant j \leqslant n, x_{j\alpha}, x_{j\beta} : \Re \to \Re$ are the states, $\vec{v}_s^{\alpha\beta} = [v_s\ 0]^T$ is the system input which is the extension to $\Re^2$ of $v_s, \vec{v}_{sf}^{\alpha\beta} = [v_{sf\alpha}\ v_{sf\beta}]^T$ is the output vector of the system, $v_{sf\alpha}, v_{sf\beta} : \Re \to \Re, |\vec{v}_{sf}^{\alpha\beta}|^2 = \vec{v}_{sf}^{\alpha\beta^T}\vec{v}_{sf}^{\alpha\beta}$, and finally $a_j, c_j, \tau \in \Re, 1 \leqslant j \leqslant n$ are design constants. The design rules for the constants are presented along the next section, and resumed in Section III-C.

The proposed structure corresponds to a linear time-varying system where $\bar{\omega}$ is the (unique) slowly varying parameter, permanently adapted by (2).

To better visualize the system structure, the system (1)–(3) are written here for the case $n = 1$

$$\begin{bmatrix} \dot{x}_{1\alpha} \\ \dot{x}_{1\beta} \end{bmatrix} = -a_1 \begin{bmatrix} x_{1\alpha} \\ x_{1\beta} \end{bmatrix} + \bar{\omega} \begin{bmatrix} -x_{1\beta} \\ x_{1\alpha} \end{bmatrix} + \begin{bmatrix} v_s \\ 0 \end{bmatrix} \qquad (5)$$

$$\begin{bmatrix} v_{sf\alpha} \\ v_{sf\beta} \end{bmatrix} = c_1 \begin{bmatrix} x_{1\alpha} \\ x_{1\beta} \end{bmatrix} \qquad (6)$$

$$\dot{\hat{\omega}} = \frac{1}{\tau}\left(-\hat{\omega} + \frac{x_{1\alpha}\dot{x}_{1\beta} - x_{1\beta}\dot{x}_{1\alpha}}{x_{1\alpha}^2 + x_{1\beta}^2}\right) \qquad (7)$$

$$\bar{\omega} = sat(\hat{\omega}). \qquad (8)$$

Note that the derivatives involved in (2) are algebraically computed from (1). So no derivative action is needed to implement the algorithm, an important advantage for digital implementations.

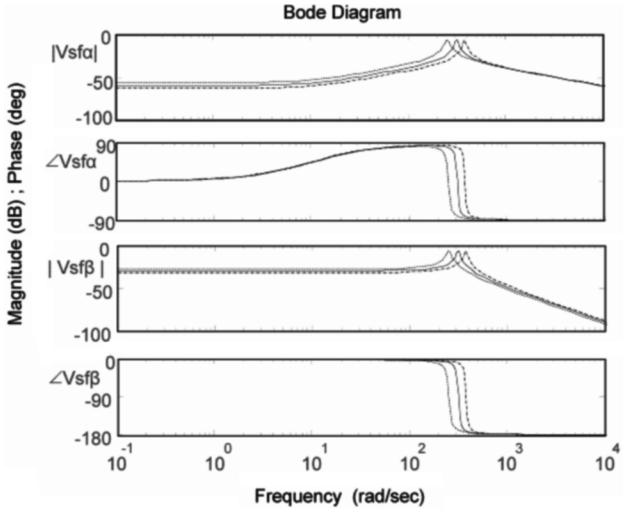

Fig. 1. Bode diagram of the reduced-order system outputs (dash: $\omega = 80\pi$, solid: $\omega = 100\pi$, dash-dot: $\omega = 120\pi$).

III. System Analysis

A first simple analysis is done on the reduced system (5)–(7) considering that the frequency $\bar{\omega} = \hat{\omega}$ (that is, the saturation (8) is working in the linear zone). The objective is to understand the behavior of circuit showing the mechanism that produces the frequency tracking, prior to the development of the stability proof of the general system.

First note that the particular structure of (5)–(6) for constant $\bar{\omega}$ corresponds to a second order linear system whose eigenvalues are $-a_1 \pm j\bar{\omega}$, where the natural resonance frequency is $\bar{\omega}$. The input-output behavior corresponds to a pass band filter tuned at the central frequency $\bar{\omega}$. The driving signal v_s is periodic with fundamental frequency $\omega \approx \bar{\omega}$ and possibly with higher order harmonic components and/or nonzero mean value. Fig. 1 shows as example the magnitude and phase response of the simple system (5)–(6) for $a_1 = 10, c_1 = 20$ and for the frequency set $\bar{\omega} = \{80\pi, 100\pi, 120\pi\}$. The harmonic components, and the possible existing dc component of the driving signal are highly attenuated at the filter outputs (6), which, in steady state, contains mainly the fundamental frequency component, amplified and phase-shifted accordingly to the filter response. In particular, the phase of the output signal $v_{sf\beta}$ falls abruptly from zero to -180 degrees while the frequency of the input signal sweeps from below to above $\bar{\omega}$, being exactly -90 degrees when the system is tuned at the driving frequency.

This implies that when the frequency $\bar{\omega} > \omega$ then the phase shift of $v_{sf\beta}$ belongs to the open interval $(-90, 0)$ degrees, and when $\bar{\omega} < \omega$ the phase-shift of $v_{sf\beta}$ belongs to the open interval $(-180, -90)$ degrees.

By replacing the state derivatives (5) in the adaptation law (7) and assuming linear behavior of (8), it results in

$$\dot{\hat{\omega}} = -\frac{c_1}{\tau}\left(\frac{v_{sf\beta}v_s}{v_{sf}^T v_{sf}}\right). \qquad (9)$$

Being c_1/τ small enough, then the adaptation law (9) for $\bar{\omega}$ will respond in average to the mean value of the factor between brackets. This mean value is positive for $\bar{\omega} > \omega$ and negative

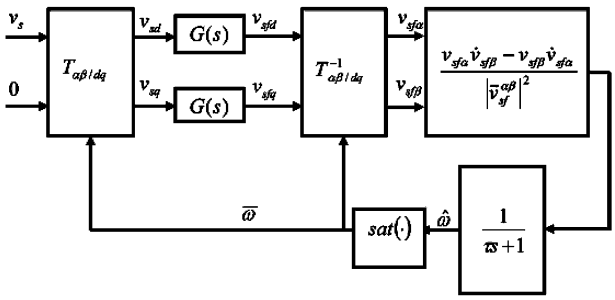

Fig. 2. Block diagram of the system described by (1)–(4).

for $\bar{\omega} < \omega$ (due to the phase-shift in each case), which forces $\bar{\omega}$ to move into a small bounded neighborhood of ω. For this, remember that in steady state the fundamental frequency present at the output $v_{sf\beta}$ is ω, and all products between $v_{sf\beta}$ and the dc- or harmonic components of the input signal have zero mean value.

Turning back to the full order system (1)–(3), it is better analyzed if expressed in a rotating frame synchronized with $\bar{\omega}t$. For that the variables of the system (1)–(2) referred to a stationary orthonormal reference frame $\alpha\beta$ are transformed to express them with respect to another orthonormal dq frame whose axis d is rotated $\bar{\omega}t$ radians with respect to the axis α. The adequate transformation matrix is

$$T_{\alpha\beta/dq} = \begin{bmatrix} \cos(\bar{\omega}t) & \sin(\bar{\omega}t) \\ -\sin(\bar{\omega}t) & \cos(\bar{\omega}t) \end{bmatrix}. \tag{10}$$

By changing variables in (1), $\vec{x}_j^{\alpha\beta} = T^{-1}_{\alpha\beta/dq}\vec{x}_j^{dq}, \vec{v}_{sf}^{\alpha\beta} = T^{-1}_{\alpha\beta/dq}\vec{v}_{sf}^{dq} 1 \leqslant j \leqslant n$, and considering that $\dot{T}^{-1}_{\alpha\beta/dq} = \bar{\omega}PT^{-1}_{\alpha\beta/dq}$, the system is rewritten as

$$\begin{aligned} \dot{\vec{x}}_k^{dq} &= \vec{x}_{k+1}^{dq}, \quad 1 \leqslant k \leqslant n-1 \\ \dot{\vec{x}}_n^{dq} &= -a_1\vec{x}_1^{dq} - \cdots - a_n\vec{x}_n^{dq} + \vec{v}_s^{dq} \\ \vec{v}_{sf}^{dq} &= c_1\vec{x}_1^{dq} + \cdots + c_n\vec{x}_n^{dq} \end{aligned} \tag{11}$$

where $\vec{x}_j^{dq} = [x_{jd}\ x_{jq}]^T, 1 \leqslant j \leqslant n, \vec{v}_s^{dq} = [v_{\rm sd}\ v_{sq}]^T$ and $\vec{v}_{sf}^{dq} = [v_{sfd}\ v_{sfq}]^T$.

In the new reference frame, the dependence of the system equations with $\bar{\omega}$ is not explicit since now it is taken into account by (10). From (11), it is clear that the system described by (1)–(3) is functionally equivalent to that shown in the block diagram of Fig. 2, where $G(s)$ is

$$G(s) = \frac{c_n s^{n-1} + c_{n-1}s^{n-2} + \cdots + c_1}{s^n + a_n s^{n-1} + \cdots + a_1}. \tag{12}$$

The so-obtained block diagram induces an heuristic justification of the system behavior. For it, first assume that $\hat{\omega}$ remains between the saturation limits defined for (3), which it allows rewriting (2) as

$$\dot{\hat{\omega}} = \frac{1}{\tau}\left(-\bar{\omega} + \frac{v_{sf\alpha}\dot{v}_{sf\beta} - v_{sf\beta}\dot{v}_{sf\alpha}}{|\vec{v}_{sf}^{\alpha\beta}|^2}\right). \tag{13}$$

Then, the variables in (13) are also transformed to the dq frame. First observe that $v_{sf\alpha}\dot{v}_{sf\beta} - v_{sf\beta}\dot{v}_{sf\alpha}$ in (13) coincides with $-v_{sf}^{\alpha\beta T} P \dot{v}_{sf}^{\alpha\beta}$. Then, apply the already-defined change of variables $\vec{v}_{sf}^{\alpha\beta} = T^{-1}_{\alpha\beta/dq}\vec{v}_{sf}^{dq}$, recalling that $|\vec{v}_{sf}^{\alpha\beta}| = |\vec{v}_{sf}^{dq}|, \dot{T}^{-1}_{\alpha\beta/dq} = \bar{\omega}PT^{-1}_{\alpha\beta/dq}, T^{-1^T}_{\alpha\beta/dq} = T_{\alpha\beta/dq}$, $T_{\alpha\beta/dq}PT^{-1}_{\alpha\beta/dq} = P$, and $PP = -I^{2\times 2}$ (where $I^{2\times 2}$ is the identity matrix of second order). The transformed version of (13) is

$$\dot{\hat{\omega}} = \frac{1}{\tau}\frac{v_{sfd}\dot{v}_{sfq} - v_{sfq}\dot{v}_{sfd}}{|\vec{v}_{sf}^{dq}|^2}. \tag{14}$$

Considering that the vector $\vec{v}_{sf}^{dq}$ is rotated θ radians with respect to the axis d, this last equation shows an important fact: If $\vec{v}_{sf}^{dq}$ varies, the right hand side of (14) represents the angular velocity of the vector in the rotating reference frame dq, as explained in the sequel. To visualize this fact, observe that θ is given by $\theta = \arctan(v_{sfd}/v_{sfq})$. Recalling that $D\left[\arctan(u)\right] = D[u]/(1+u^2)$ (being D the derivative operator) results in

$$\dot{\theta} = D[\arctan(v_{sfd}/v_{sfq})] = \frac{v_{sfd}\dot{v}_{sfq} - v_{sfq}\dot{v}_{sfd}}{|\vec{v}_{sf}^{dq}|^2} \tag{15}$$

which coincides with (14). This means that the time derivative of $\bar{\omega}$ in (14) is proportional to the angular velocity of $\vec{v}_{sf}^{dq}$ in the considered rotating reference frame. As a consequence, if $\vec{v}_{sf}^{dq}$ is rotating in the clockwise direction (in the dq reference frame), the system (1)–(3) acts to increase the value of $\bar{\omega}$, and consequently, the speed of the dq reference frame, and vice-versa. The system forces $\bar{\omega}$ to change in such a way that the magnitude of the angular velocity of $\vec{v}_{sf}^{dq}$ is reduced with respect to the rotating reference frame. This fact explains the behavior of the system. Moreover, assuming that: 1) the voltage $\vec{v}_{sf}^{dq}$ converges to a vector of *constant amplitude* and 2) the system is able to reduce practically to zero the angular velocity of $\vec{v}_{sf}^{dq}$ with respect to the frame dq, in such a way that $\bar{\omega} \to \omega$ (constant); then from the structure of $T^{-1}_{\alpha\beta/dq}$ it is easy to understand that the output of the system $\vec{v}_{sf}^{\alpha\beta} = T^{-1}_{\alpha\beta/dq}\vec{v}_{sf}^{dq}$ is a vector conformed by two high-quality sinusoidal signals. Those two assumptions are addressed in the next two subsections.

A. Proof that $\vec{v}_{sf}^{d'q'}$ Converges to a Constant Value

Here, we assume that the second assumption is true: $\bar{\omega}$ converges to a constant value near ω (this assumption will be discarded in the next subsection). Then, we prove here that the first assumption holds: Voltage $\vec{v}_{sf}^{dq}$ converges to constant amplitude vector.

For the general case of the input to the system (Fig. 2) having harmonic components, it can be written that

$$\begin{bmatrix} v_s \\ 0 \end{bmatrix} = \sum_{k\geqslant 1}\frac{1}{2}\left(V_{\rm sk}\begin{bmatrix} \cos(k\omega t + \varphi_k) \\ \sin(k\omega t + \varphi_k) \end{bmatrix} + V_{\rm sk}\begin{bmatrix} \cos(-k\omega t - \varphi_k) \\ \sin(-k\omega t - \varphi_k) \end{bmatrix}\right) \tag{16}$$

where V_{sk} is the amplitude of the kth harmonic component of v_s and φ_k is its relative phase. The dc component of the input signal will not be considered here, but it is easy to prove by the

same arguments that follow that the system is also able to deal with this component.

The last particular way of writing the input signal leads to see each component of the extension to $\Re^2$ of v_s as formed by the sum of two rotating vector components of frequency $k\omega$, one with positive sequence and the other with negative sequence. Clearly, the output of block $T_{\alpha\beta/dq}$ in Fig. 2 will be composed by the sum of all positive and negative sequence vectors having frequencies $k\omega - \bar{\omega}$ as follows:

$$\begin{aligned}\vec{v}_s^{dq} = \begin{bmatrix} v_{\rm sd} \\ v_{sq} \end{bmatrix} &= \frac{V_{s1}}{2}\begin{bmatrix} \cos[(\omega-\bar{\omega})t+\varphi_1] \\ \sin[(\omega-\bar{\omega})t+\varphi_1]\end{bmatrix} \\ &+ \frac{V_{s1}}{2}\begin{bmatrix} \cos[(-\omega-\bar{\omega})t-\varphi_1] \\ \sin[(-\omega-\bar{\omega})t-\varphi_1]\end{bmatrix} \\ &+ \sum_{k>1}\frac{1}{2}\left(V_{sk}\begin{bmatrix} \cos[(k\omega-\bar{\omega})t+\varphi_k] \\ \sin(k\omega-\bar{\omega})t+\varphi_k]\end{bmatrix}\right. \\ &\left. + V_{sk}\begin{bmatrix} \cos[(-k\omega-\bar{\omega})t-\varphi_k] \\ \sin(-k\omega-\bar{\omega})t-\varphi_k]\end{bmatrix}\right). \end{aligned} \tag{17}$$

In this last expression, for the sake of clarity, the vector corresponding to the fundamental frequency of v_s was separately written.

Assuming that the transfer function $G(s)$ is exponentially stable by design, and considering that the saturation block causes the frequency $\bar{\omega}$ to remain in a bounded neighborhood of ω (remember also that for the moment the assumption of $\bar{\omega} \to \omega$ (constant) holds), the vector $\vec{v}_{sf}^{dq}$, output of the transfer function $G(s)$ (see Fig. 2), can be written in the steady state as follows

$$\begin{aligned}\vec{v}_{sf}^{dq} &= V'_{s1}\begin{bmatrix} \cos[(\omega-\bar{\omega})t+\varphi'_1] \\ \sin[(\omega-\bar{\omega})t+\varphi'_1]\end{bmatrix} \\ &+ V'_{s-1}\begin{bmatrix} \cos[(-\omega-\bar{\omega})t+\varphi''_1] \\ \sin[(-\omega-\bar{\omega})t+\varphi''_1]\end{bmatrix} \\ &+ \sum_{k>1}\left(V'_{sk}\begin{bmatrix} \cos[(k\omega-\bar{\omega})t+\varphi'_k] \\ \sin(k\omega-\bar{\omega})t+\varphi'_k]\end{bmatrix}\right. \\ &\left. + V'_{s-k}\begin{bmatrix} \cos[(-k\omega-\bar{\omega})t+\varphi''_k] \\ \sin(-k\omega-\bar{\omega})t+\varphi''_k]\end{bmatrix}\right) \end{aligned} \tag{18}$$

where $V'_{sk} = |G[j(k\omega - \bar{\omega})]|V_{sk}/2, k \in \boldsymbol{N}$ and φ'_k, φ''_k are the phase of the components of the output signal, $\varphi'_k = \varphi_k + \arg\{G[j(k\omega - \bar{\omega})]\}$, $\varphi''_k = -\varphi_k + \arg\{G[j(-k\omega - \bar{\omega}]\}$. Observe that the first term of (18) is a low frequency vector (of $(\omega - \bar{\omega})$ rad/s), and the remaining terms have frequencies that are $(k-1)\omega$ rad/s higher, for $k \in \boldsymbol{N}$.

If G(s) is designed to be a low-pass filter with small enough cutoff frequency then $V'_{s1} > V'_{sk}$ since $|G(j(\omega - \bar{\omega}))|V_{s1} > |G(j(k\omega - \bar{\omega}))|V_{sk}$ for $k > 1$, which means that the $\mathrm{THD}_v\%$ of (18) is smaller than the $\mathrm{THD}_v\%$ of (17). For $\omega \to \bar{\omega}, G(j(\omega - \bar{\omega})) \to G(0)$ and $G(j(k\omega - \bar{\omega})) \to G(j(k-1)\omega) \leqslant G(j\omega) < G(0)$. If the attenuation of $G(\cdot)$ is high enough in the stopband, all terms of $\vec{v}_{sf}^{dq}$ in (18) will vanish except the first one.

If $G(0) = 2$, and the magnitude of $G(s)$ is reasonably constant until its cutoff frequency, the magnitude of vector $\vec{v}_{sf}^{dq}$ will be similar to the magnitude of vector V_{s1}. The difference between the magnitudes of these two vectors is proportional to the difference between $|G(\omega - \bar{\omega})|$ and $G(0)$. The maximum value of $G(\omega - \bar{\omega})$, for $\omega_{\min} \leqslant \bar{\omega} \leqslant \omega_{\max}$ and $\omega_{\min} \leqslant \omega \leqslant \omega_{\max}$, can be kept bounded by designing $G(s)$ properly. The magnitude of all the remaining terms of (18) will be lower than the magnitude of the first one. In compact form, (18) is rewritten as

$$\vec{v}_{sf}^{dq} = V'_{s1}\begin{bmatrix} \cos[(\omega-\bar{\omega})t+\varphi'_1] \\ \sin[(\omega-\bar{\omega})t+\varphi'_1]\end{bmatrix} + \begin{bmatrix} e_d \\ e_q \end{bmatrix} \tag{19}$$

where $\vec{e}^{dq} = [e_d \;\; e_q]^T$ is a vector that collects together all the terms of $\vec{v}_{sf}^{dq}$ except the first one. This resulting vector is composed by a sum of rotating vectors whose velocity is $k\omega - \bar{\omega}$, with $k \leqslant -1, k > 1$, and $|\vec{e}^{dq}| << V'_{s1}$.

The settling time of $\vec{v}_{sf}^{dq}$ to the value given by (19) depends on the bandwidth of $G(s)$. For example, consider an application where a 50-Hz sinusoidal signal has to be extracted. If it is required to have high speed in the response of the system output to changes in the input, this transfer function could be chosen to be a fifth order elliptic low-pass filter with cutoff frequency of 20 Hz, maximum attenuation of 1 dB in the passband region, and minimum attenuation of 60 dB in the stopband region, which assures a small enough ripple on v_{sf}^{dq} with a fast enough transient response. If it is not required high speed in the response, a single first-order low-pass filter could be chosen.

Convergence of $\vec{v}_{sf}^{dq}$ to a predominant low frequency waveform with low-amplitude harmonic components is assured by designing adequately $G(s)$ and the saturation limits in (3)–(4) (assuming $\bar{\omega}$ constant and v_s with harmonic components upper bounded in magnitude). Observe that if it were proved that $\bar{\omega}$ converges to ω, then it would be assured that (19) converges to an almost constant value and that the output of the system $\vec{v}_{sf}^{\alpha\beta} = T^{-1}_{\alpha\beta/dq}\vec{v}_j^{dq}$ would converge to a vector composed by high quality sinusoidal signals. This convergence of $\bar{\omega}$ will be addressed in the next subsection.

B. Proof that $\bar{\omega}$ Converges to a Constant Value of Nearly ω

It remains to analyze the convergence of $\bar{\omega}$ to ω. Up to now, it was considered $\bar{\omega}$ as constant to obtain (19). It is convenient to use (14) to analyze the variations of $\bar{\omega}$. The values of $\dot{\vec{v}}_{sf}^{dq} = [\dot{v}_{sd} \;\; \dot{v}_{sq}]^T$ are computed using (18) as follows:

$$\begin{aligned}&\dot{\vec{v}}_{sf}^{dq} \\ &= (\omega-\bar{\omega})V'_{s1}\begin{bmatrix} -\sin[(\omega-\bar{\omega})t+\varphi'_1] \\ \cos[(\omega-\bar{\omega})t+\varphi'_1]\end{bmatrix} \\ &+ (-\omega-\bar{\omega})V'_{s-1}\begin{bmatrix} -\sin[(-\omega-\bar{\omega})t+\varphi'_1] \\ \cos[(-\omega-\bar{\omega})t+\varphi'_1]\end{bmatrix} \\ &+ \sum_{k>1}\left((k\omega-\bar{\omega})V'_{sk}\begin{bmatrix} -\sin[(k\omega-\bar{\omega})t+\varphi'_k] \\ \cos(k\omega-\bar{\omega})t+\varphi'_k]\end{bmatrix}\right. \\ &\left. + (-k\omega-\bar{\omega})V'_{s-k}\begin{bmatrix} -\sin[(-k\omega-\bar{\omega})t+\varphi'_k] \\ \cos(-k\omega-\bar{\omega})t+\varphi'_k]\end{bmatrix}\right) + \eta \end{aligned} \tag{20}$$

where η collects all the terms which are dependent on $\dot{\omega} - \dot{\bar{\omega}}$, and its magnitude is assumed negligible compared to $\dot{\vec{v}}_{sf}^{dq}$. It is easy to find a set of positive constant values v_k, which depend on V'_{sk} and $G(s)$ [that is, a strict proper transfer function as seen

from (12)], such that they are upper bounds (at $k\omega - \bar{\omega}$) for the products $(k\omega - \bar{\omega})V'_{sk} = (k\omega - \bar{\omega})|G[j(k\omega - \bar{\omega})]|V_{sk}/2 < \nu_k, k \leqslant -1,\ k > 1$.

So, the last equation is rewritten as

$$\vec{v}_{sf}^{dq} = (\omega - \bar{\omega})V'_{s1}\begin{bmatrix} -\sin[(\omega - \bar{\omega})t + \varphi'_1] \\ \cos[(\omega - \bar{\omega})t + \varphi'_1] \end{bmatrix} + \begin{bmatrix} e'_d \\ e'_q \end{bmatrix} \quad (21)$$

where $\vec{e}'^{dq} = [e'_d\ e'_q]^T$ is a bounded vector composed by the sum of a series of bounded vectors rotating with frequency $k\omega - \bar{\omega}, k \leqslant -1, k > 1$, such that $|\vec{e}'^{dq}| << V'_{s1}$, plus η. The sum is naturally convergent due to the low-pass characteristics of $G(\cdot)$ and the convergence of (18).

Using (19) and (21) in (14), and considering that $|\vec{v}_{sf}^{dq}|^2 \approx V'^2_{s1}$ [since $|\vec{e}'^{dq}| << V'_{s1}$ in (19)], we arrive at

$$\frac{v_{sfd}\dot{v}_{sfq} - v_{sfq}\dot{v}_{sfd}}{\left|\vec{v}_{sf}^{dq}\right|^2} = (\omega - \bar{\omega}) + o(t) \quad (22)$$

where $o(t)$ represents a bounded function, whose magnitude is defined by the attenuation of $G(s)$ in the passband and by the harmonic components of the input. It is noted that this function could have nonzero mean value, as can be verified by calculating the products in (22). Replacing (22) in (14), for $|\omega - \bar{\omega}| > \max\{o(t)\}$, it results that the sign of the time variation in $\bar{\omega}$ is equal to the sign of $\omega - \bar{\omega}$. This implies that if $\omega > \bar{\omega}$ the trend is to increase $\bar{\omega}$ and vice versa.

Equation (22) was obtained under the assumption of convergence of the internal variables of $G(s)$ considering that $\bar{\omega}$ is constant. To justify the convergence of $\bar{\omega}$ to ω, it will be assumed that $\bar{\omega}$ is a slowly varying parameter with respect to the speeds of variation of all system variables in (22). The dynamics of $\bar{\omega}$ is specified by parameter τ (with units of time) in (14). Its value is chosen high enough as to distinguish the dynamics of $\bar{\omega}$ from those of other system variables using the theory of singular perturbations [12], which leads to a great simplification of the stability analysis of nonlinear dynamic systems. Based on that selection of τ, it is assumed that all variables except $\bar{\omega}$ have converged, so that the dynamics of $\bar{\omega}$ can be computed from (22). The assumption of slow variation of $\bar{\omega}$ does not imply any limitation for the application of the proposed system to active power filters since the line frequency is a slow varying parameter.

From (14) and (22), and considering the ω constant, it is seen that the error dynamics $e_\omega = \bar{\omega} - \omega$, described by

$$\dot{\bar{\omega}} = \dot{\bar{\omega}} - \dot{\omega} = \dot{e}_\omega = -\frac{1}{\tau}[e_\omega + o(t)] \quad (23)$$

is such that the magnitude of the error $e_\omega = \bar{\omega} - \omega$ is bounded. This is shown below.

Defining $V = e_\omega^2/2$ as a Lyapunov function candidate, its time derivative results in

$$\dot{V} = e_\omega\dot{e}_\omega = -e_\omega^2\frac{1}{\tau} + \frac{1}{\tau}e_\omega o < 0, \quad \text{for } |e_\omega| > o \quad (24)$$

which means that the function $V = e_\omega^2$ decreases for $|e_\omega| > |o(t)|$, so that $|e_\omega|$ is kept upper bounded by o. As a consequence, $V'_{s1} \to V_{s1}$ and $\varphi'_1 \to \varphi_1$ since $G(0) = 2$ in the first term of (18). Neglecting the other high-frequency terms (because they are highly attenuated by $G(s)$) results in

$$\vec{v}_{sf}^{dq} \approx V_{s1}\begin{bmatrix} \cos[(\omega - \bar{\omega})t + \varphi_1] \\ sen[(\omega - \bar{\omega})t + \varphi_1] \end{bmatrix} \quad (25)$$

and the output of the block $T^{-1}_{\alpha\beta/dq}$ in Fig. 2 is

$$\vec{v}_{sf}^{\alpha\beta} \approx V_{s1}\begin{bmatrix} \cos[(\omega)t + \varphi_1] \\ \text{sen}[(\omega)t + \varphi_1] \end{bmatrix} \quad (26)$$

which is the positive sequence component at the fundamental frequency of the extension to $\Re^2$ of v_s, obtained practically without amplitude or phase error.

Furthermore, the two components of the output (26) are shifted $\pi/2$ radians so both outputs can be used to implement the transformation used in active power filter controllers that work in the $\alpha\beta$ reference frame.

C. Design Rules

The design parameters are $a_j, c_j, \tau \in \Re, 1 \leqslant j \leqslant n$. The design rules for them were presented along the previous section, and are summarized below.

- Parameters $a_j, c_j, 1 \leqslant j \leqslant n$ define $G(s)$ as in (12) which must be designed as an exponentiallly stable low-pass filter with $G(0) = 2$, and $|G(s)|$ with high enough attenuation in the stopband. The bandwidth of G (s) must be chosen to keep the first term of (18) within the passband and the remaining terms within the stopband. The attenuation in the stopband of G (s) determines the quality of the output signal ($\text{THD}_v\%$). Higher attenuation means lower $\text{THD}_v\%$. The settling time of the filter output depends on the bandwidth of $G(s)$. Wider bandwidth means shorter settling time and higher sensitivity to perturbations on the input waveform frequency and phase.
  Parameter τ defines the time constant of the first-order error dynamics (23) and its value is chosen high enough as to distinguish the dynamics of $\bar{\omega}$ from those of other system variables.

D. Remarks

It was proven that the system (1)–(4) is able to asymptotically determine the fundamental frequency component of a periodic input signal with negligible amplitude and phase error, even when the frequency of the input signal has slow and bounded variations. These characteristics are not easy to obtain by using a standard bandpass filter, and it is harder when its transition band is narrower.

The system (1)–(4) provides an output which is in phase with the system input so it behaves like a PLL and can be used as its replacement in some classical active filter designs (see [8]) where the line voltage is the input. A clear advantage is to avoid the need of look-up tables for the evaluation of the sine function

(the quality of the obtained sine signal degrades if the table is not long enough) and all the components associated to the PLL (VCO, filters, etc.).

To obtain a three-phase balanced output, it is enough to multiply the output $\vec{v}_{sf}^{\alpha\beta} = [v_{sf\alpha}\ \ v_{sf\beta}]^T$ by the following gain matrix:

$$T_{3/2} = \begin{bmatrix} 1 & 0 \\ -\frac{1}{2} & \frac{\sqrt{3}}{2} \\ -\frac{1}{2} & -\frac{\sqrt{3}}{2} \end{bmatrix} \tag{27}$$

which transforms a vector in the $\alpha\beta$ frame, into other vector expressed with respect to the frame abc with null zero-sequence components, and whose module is $\sqrt{3/2}$ times greater.

An alternative use of (1)–(4) appears from an analysis of (26), which it is to replace the standard band-pass filters used in active filtering applications [9]. The proposed system is not affected by the amplitude and phase errors present in those filters under frequency variations when designed for sharp cutoff frequencies. For other cases, this strategy can extract accurately the $\sin(\omega t)$ and $\cos(\omega t)$ signals needed for implementation of notch filters used in unbalance rejection algorithms embedded in the controllers of active magnetic bearings [13]. It is only necessary to measure any periodic signal of the system with fundamental frequency ω.

IV. Discretization Issues

This section shows the discrete version of system (1)–(3) for the case $n = 1$ (useful for real-time applications) to illustrate the practical implementation problems and the applied simplifications.

Observe that the system (1)–(4) is nonlinear since (1) contains the product of states $\bar{\omega}$ and $\vec{x}_1^{\alpha\beta}$, which are nonlinearly related by (3). The fact that $\bar{\omega}$ is a slowly varying parameter enables to consider (1)–(3) as a discrete system where $\bar{\omega}(h) \approx \bar{\omega}(h-1)$, with h being the sample number. This allows to consider (1) as a linear time-varying system, with $\bar{\omega}$ as the varying parameter, being $\bar{\omega}\,(h-1)$ its value in the time interval h (that is not affected by variations of $\vec{x}_1^{\alpha\beta}$ during that cycle). This approximation would require the discrete realization of (1) interval by interval for each different value of $\bar{\omega}\,(h-1)$. To avoid this cumbersome work, it is chosen to use a discrete integrator.

It was verified by computer simulations that using a forward- Euler method for the discrete integrator (without direct feedthrough) required a much higher sampling frequency than a trapezoidal method to attain the same numerical errors in the steady-state output (the benefits of using a trapezoidal integration method are explained in [14]). So, a trapezoidal method was chosen (with direct feedthrough, such as $y(h) = y(h-1) + (T_s/2)[u(h) + u(h-1)]$, where y, u are the input and output of the integrator, and T_s is the sampling time) to approximate the integrals in the system (1). The chosen integration method was adequate for typical sampling rates within the range between 5 to 10 kHz and for inputs with fundamental line frequency component.

Based on the above, the discrete system becomes

$$\begin{aligned} &\begin{bmatrix} x_{1\alpha}(h) \\ x_{1\beta}(h) \end{bmatrix} \\ &\quad = \begin{bmatrix} x_{1\alpha}(h-1) \\ x_{1\beta}(h-1) \end{bmatrix} + \frac{T_s}{2}\left\{-a_1 \begin{bmatrix} x_{1\alpha}(h) \\ x_{1\beta}(h) \end{bmatrix} \right. \\ &\qquad \left. + \bar{\omega}(h-1) \begin{bmatrix} -x_{1\beta}(h) \\ x_{1\alpha}(h) \end{bmatrix} + \begin{bmatrix} v_s(h) \\ 0 \end{bmatrix}\right\} \\ &\qquad + \frac{T_s}{2}\left\{-a_1 \begin{bmatrix} x_{1\alpha}(h-1) \\ x_{1\beta}(h-1) \end{bmatrix} \right. \\ &\qquad \left. + \bar{\omega}(h-2) \begin{bmatrix} -x_{1\beta}(h-1) \\ x_{1\alpha}(h-1) \end{bmatrix} + \begin{bmatrix} v_s(h-1) \\ 0 \end{bmatrix}\right\}. \end{aligned} \tag{28}$$

Observe from the last equation that the next state $\vec{x}_1^{\alpha\beta}(h)$ is used in both sides of the equation because of the use of the integrator with direct feedthrough.

Moving to the left-hand side the term with $\vec{x}_1^{\alpha\beta}(h)$ and rearranging yields the following equivalent equation:

$$\begin{aligned} &\begin{bmatrix} 2/T_s + a_1 & \bar{\omega}(h-1) \\ -\bar{\omega}(h-1) & 2/T_s + a_1 \end{bmatrix} \begin{bmatrix} x_{1\alpha}(h) \\ x_{1\beta}(h) \end{bmatrix} \\ &\quad = \begin{bmatrix} 2/T_s - a_1 & -\bar{\omega}(h-2) \\ \bar{\omega}(h-2) & 2/T_s - a_1 \end{bmatrix} \begin{bmatrix} x_{1\alpha}(h-1) \\ x_{1\beta}(h-1) \end{bmatrix} \\ &\qquad + \begin{bmatrix} v_s(h) - v_s(h-1) \\ 0 \end{bmatrix}. \end{aligned} \tag{29}$$

Computing the inverse of the matrix on the left hand side and premultiplying both sides, the following discrete system results:

$$\begin{aligned} &\begin{bmatrix} x_{1\alpha}(h) \\ x_{1\beta}(h) \end{bmatrix} \\ &\quad = D(h-1)\left\{\begin{bmatrix} A(h-1) & -B(h-1) \\ B(h-1) & A(h-1) \end{bmatrix} \begin{bmatrix} x_{1\alpha}(h-1) \\ x_{1\beta}(h-1) \end{bmatrix} \right. \\ &\qquad \left. + \begin{bmatrix} C \\ \bar{\omega}(h-1) \end{bmatrix} [v_s(h) - v_s(h-1)]\right\} \end{aligned} \tag{30}$$

where $A(h-1) = (2/T_s + a_1)(2/T_s - a_1) - \bar{\omega}(h)\bar{\omega}(h-1), B(h-1) = (2/T_s - a_1)\bar{\omega}(h) + (2/T_s + a_1)\bar{\omega}(h-1), C = 2/T_s + a_1$ and $D(h-1) = [(2/T_s + a_1)^2 + \bar{\omega}^2(h-1)]^{-1}$.

The value of $\bar{\omega}(h-1)$ to be used in (30) is computed by $\bar{\omega}(h-1) = \mathrm{sat}[\hat{\omega}\,(h-1)]$, where $\hat{\omega}\,(h)$ (the discrete version of (2)), is obtained from the following linear filter:

$$\hat{\omega}(h) = a_\tau \tilde{\omega}(h) + b_\tau \hat{\omega}(h-1) \tag{31}$$

being a_τ, b_τ constants, obtained from the discretization of the transfer function $1/(\tau s + 1)$ used in (3) (e.g., for a zero-order sample and hold at the input), and

$$\tilde{\omega}(h) = \frac{x_{1\alpha}(h)\dot{x}_{1\beta}(h) - x_{1\beta}(h)\dot{x}_{1\alpha}(h)}{x_{1\alpha}^2(h) + x_{1\beta}^2(h)} \tag{32}$$

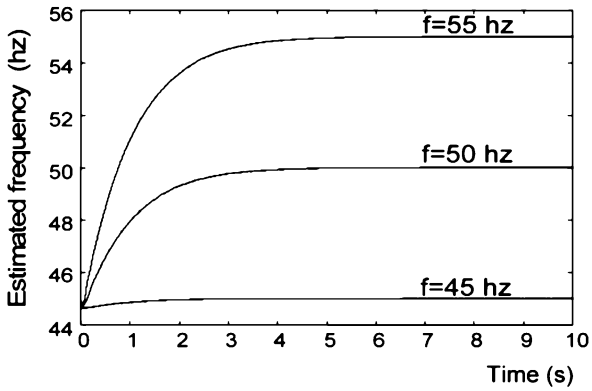

Fig. 3. Estimated frequency $\vec{\omega}\ /2\pi$ in Example 1.

$$\dot{x}_{1\alpha}(h) = [x_{1\alpha}(h) - x_{1\alpha}(h-1)]/T_s \tag{33}$$

$$\dot{x}_{1\beta}(h) = [x_{1\beta}(h) - x_{1\beta}(h-1)]/T_s. \tag{34}$$

Finally, the system output is obtained from

$$\begin{bmatrix} v_{sf\alpha}(k) \\ v_{sf\beta}(k) \end{bmatrix} = c_1 \begin{bmatrix} x_{1\alpha}(k) \\ x_{1\beta}(k) \end{bmatrix}. \tag{35}$$

Expressions (30)–(35) represent the discrete version of (1)–(3), useful for a digital implementation in real time.

The simplest version of the algorithm requires two divisions, 22 products, and 12 additions. This is approximately similar to the computational load of a nonlinear control algorithm, and perhaps a bit higher than a simple control algorithm (e.g., PI controller).

Just for comparison, a simple PLL would require at least six products, four additions, and two table entries (without considering table interpolation). Our algorithm is approximately three times more complex but does not need the table lookup procedure (saving memory space).

V. Simulation and Experimental Results

The performance of the system (1)–(4) is first analyzed by simulations, and then by laboratory experiments. The results are summarized in the following examples.

Example 1: The behavior of the system (1)–(4) is simulated for the case $n = 1$ for $a_1 = 10, c_1 = 20$ and $\tau = 1$. The chosen value of a_1 is low enough for the filter G(s) to greatly attenuate the first harmonic frequency 2ω. It is assumed that v_s is a square wave with zero mean value and peak-to-peak amplitude of 1. The signal v_s can easily be represented by (16) with appropriate values for $V_{sk}, k = 1, \ldots \infty$. The input frequency is set in three successive simulations to $\omega = 2\pi 45$ rad/s, $\omega = 2\pi 50$ rad/s, and $\omega = 2\pi 55$ rad/s. The saturation limits in (4) are set to $\omega_{\min} = 2\pi 40$ rad/s and $\omega_{\max} = 2\pi 60$ rad/s. Fig. 3 shows the initial behavior of $\bar{\omega}/2\pi$, referred as the "estimated frequency" in the figure and computed from (4), with all zero initial conditions in system (1)–(3) except for $\hat{\omega}(0) = 2\pi 45$ rad/s.

Observe in the figure that for each different frequency of the input signal the variable $\bar{\omega}/2\pi$ converges to the value of the input frequency. Fig. 4 shows the behavior of the output variables $v_{sf\alpha}$ and $v_{sf\beta}$ as well as the square-wave input for the three different input frequencies. In the three cases the outputs $v_{sf\alpha}$ and $v_{sf\beta}$ have the same amplitude of 0.636 p.u., coincident with the amplitude of the fundamental-frequency component of the square-wave input signal: $2/\pi = 0.636$ p.u. In Fig. 4 the signal $v_{sf\alpha}$ is in phase with the input signal and $v_{sf\beta}$ is shifted a quarter period with respect to $v_{sf\alpha}$ for the three different frequencies. The $\mathrm{THD}_v\%$ of $v_{sf\alpha}$ for $f = 50$ Hz was 0.7%.

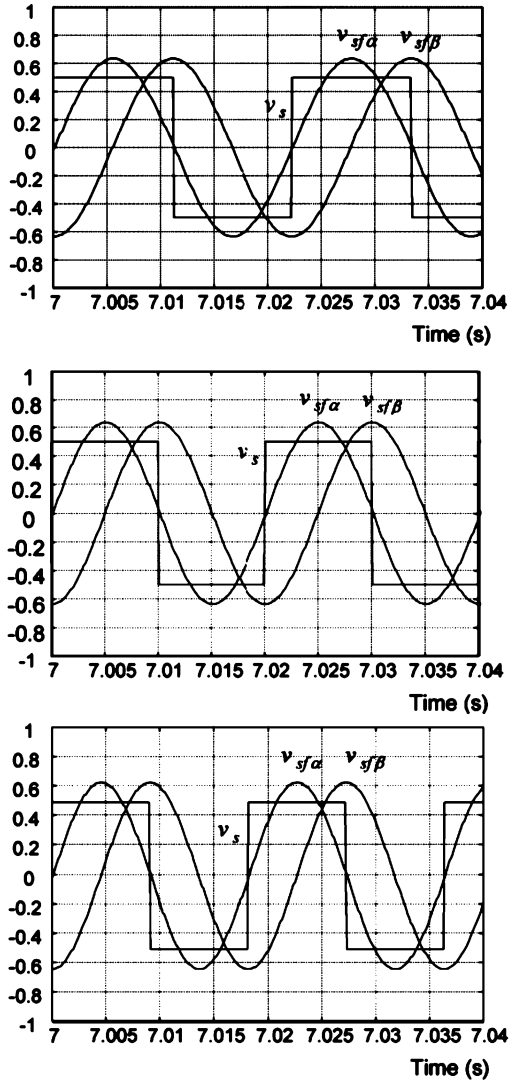

Fig. 4. Example 1: Outputs $v_{sf\alpha}$ and $v_{sf\beta}$ for $f = 45$ Hz (top), $f = 50$ Hz (middle) and $f = 55$ Hz (bottom).

Fig. 5 shows the behavior of the system when the amplitude of the input waveform is suddenly doubled (at $t = 10s$) for $\omega = 2\pi 50$ rad/s. The top figure shows the behavior of the module of the estimation of $\sqrt{v_{sf\alpha}^2 + v_{sf\beta}^2}$, which converges to the final value of 1.272 p.u., as theoretically expected. The bottom figure illustrates the behavior of the estimated frequency $\bar{\omega}/2\pi$ showing a small perturbation when the input changes its amplitude.

Fig. 6 displays in detail the estimated frequency $\bar{\omega}/2\pi$ for the case $\omega = 2\pi 50$ rad/s starting at $t = 7s$. Observe that $\bar{\omega}/2\pi$ is not constant in magnitude since its value oscillates around the

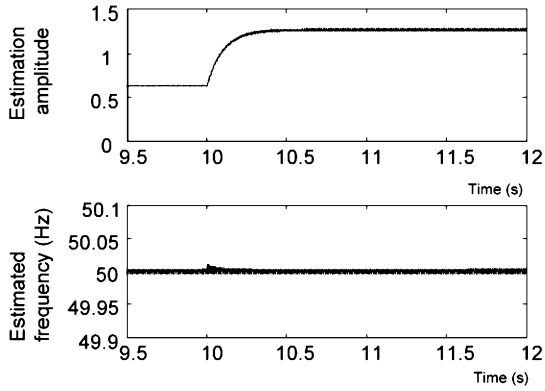

Fig. 5. Behavior of $\sqrt{v_{sf\alpha}^2 + v_{sf\beta}^2}$ (top) and estimated frequency transient (bottom) when the amplitude of the input signal in Example 1 is doubled.

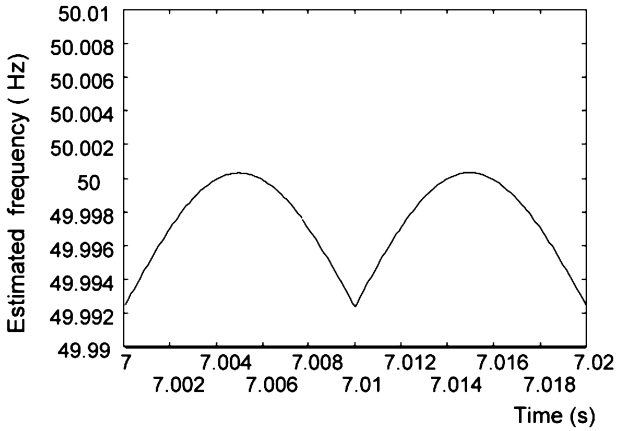

Fig. 6. Example 1: Estimated frequency $\vec{\omega}\ /2\pi$ for an input frequency of 50 Hz.

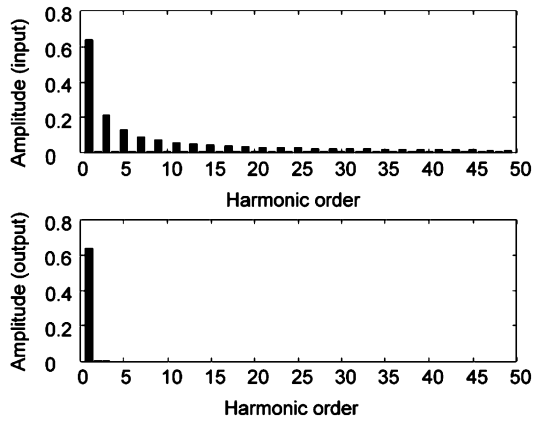

Fig. 7. Example 1: Spectrum of v_s and $v_{sf\alpha}$ (p.u.) for $\omega = 2\pi 50$ rad/s evaluated during one cycle starting at $t = 7s$.

value of the input waveform frequency. This oscillation is due to the fact that the input to the filter (3) is time varying.

Fig. 7 depicts the simulated input (v_s) and output $(v_{sf\alpha})$ signal spectrum for $\omega = 2\pi 50$ rad/s and $t = 7s$. Observe that the output signal has negligible harmonic distortion. A similar result is obtained at the other considered frequencies.

Example 2: To test the algorithm (30)-(35), the system of Example 1 ($n = 1, a_1 = 10, c_1 = 20$ and $\tau = 1$) was discretized

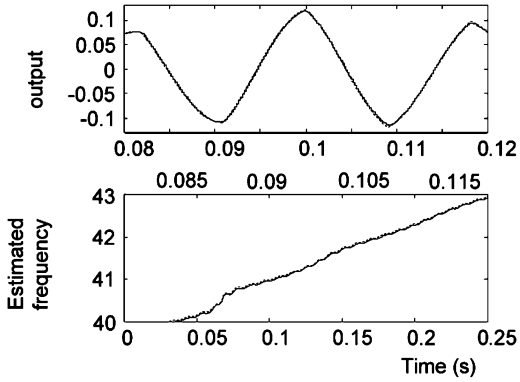

Fig. 8. Example 2: Output $v_{sf\alpha}$ (top) and estimated frequency $\vec{\omega}\ /2\pi$ (bottom), for the continuous (dashed line) and discrete simulations of the system.

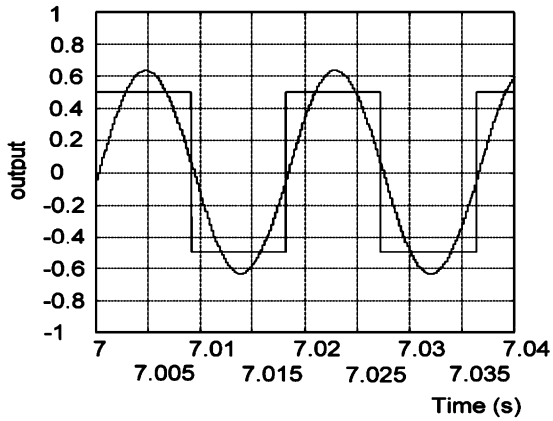

Fig. 9. Steady-state output of the discrete system (30)–(35).

using a sampling frequency of 5 kHz. The behavior of the discrete system was simulated for an input frequency of $\omega = 2\pi 55$ rad/s (used also in Example 1) with all zero initial conditions except $\hat{\omega}(0) = \omega_{\min}$. To complete the comparison, also the continuous system was simulated with a variable-step Runge-Kutta algorithm. Fig. 8 shows the behavior, predicted by the continuous and discrete simulations (the curves are superposed), of the output $v_{sf\alpha}$ and the estimated frequency $\vec{\omega}\ /2\pi$ during the initial transient period. Both simulations coincide fairly well.

Fig. 9 shows the steady-state output of the discrete system having an amplitude of 0.6358 p.u., instead of the theoretical value of $2/\pi = 0.6366$ p.u. The averaged output has a delay of one or two sampling periods. The $\mathrm{THD}_{v}\%$ of $v_{sf\alpha}$ for $f = 50$ Hz was 1.23%. The results show that (30)-(35) produce a precise enough estimation (for most practical uses) of the fundamental frequency of the input signal.

Experimental Results: The simulated system $(n = 1, a_1 = 10, c_1 = 20, \tau = 1)$ was tested experimentally, running the algorithm on a Pentium 233-MHz PC with an analog I/O board at 10 kHz (where the digital-to-analog converter had 12 b). The algorithm was written in C language and executed in real time. During the experiments a square-wave with peak-to-peak amplitude of 2 V and zero mean value was used as the input signal for these three different values of frequency: $f = 42$ Hz, $f = 50$ Hz, and $f = 57$ Hz. Fig. 10 shows the outputs $v_{s\alpha}$ and $v_{s\beta}$ that were measured using an oscilloscope. The waveform $v_{s\alpha}$

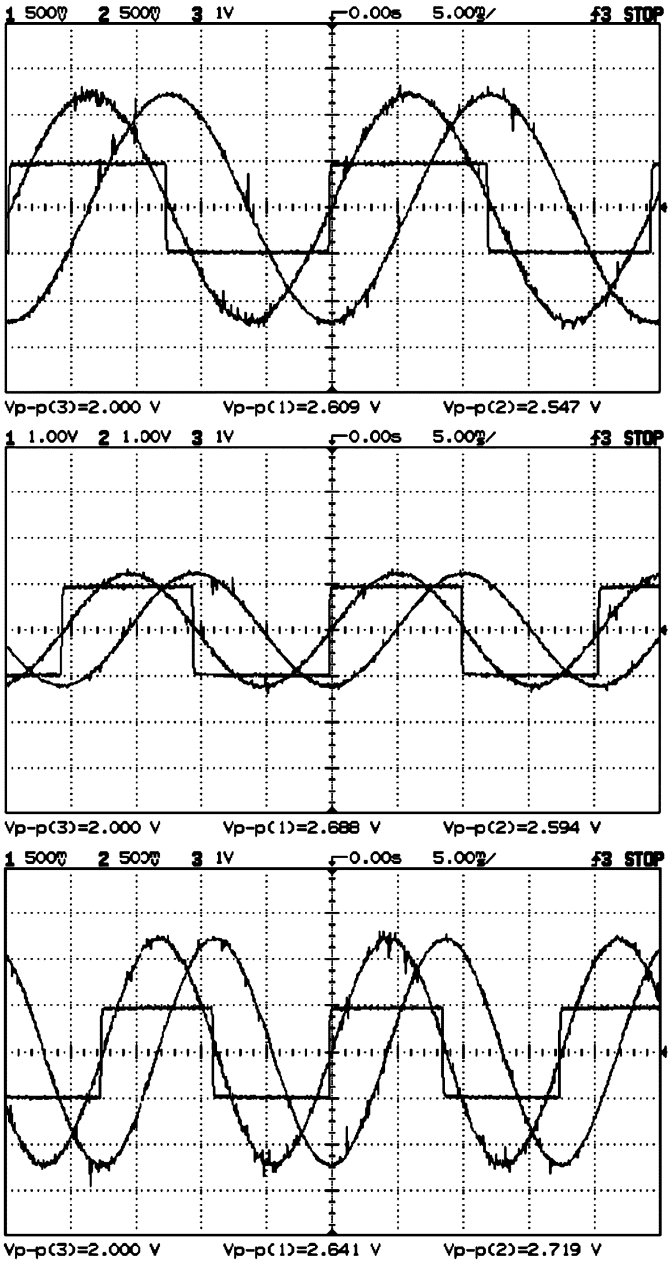

Fig. 10. Waveforms corresponding to $f = 42$ Hz (top), $f = 50$ Hz (center) and $f = 57$ Hz (bottom).

is in phase with the input waveform while $v_{s\beta}$ is a quarter period out of phase. The peak-to-peak expected value is $8/\pi = 2.5465$ V. Measurements show that the amplitude varies approximately between 2.547 and 2.719 V (some measurement noise exists), which corresponds to an error of 0.02% to 6.7% (see Fig. 10).

The frequency spectrum of the resulting waveform $v_{s\alpha}$ showed no difference with respect to the theoretical value in Example 1 so it is not included here. The $\mathrm{THD}_{v\%}$ of the resulting measured outputs was 1.9% which is a bit higher than in Example 1 due to the measurement noise (see Fig. 10).

Fig. 11 shows in detail the input waveform and $v_{s\alpha}$ when they cross through zero. The figure is scaled out for better appreciation and the zero of the vertical axis is in the middle of the figure.

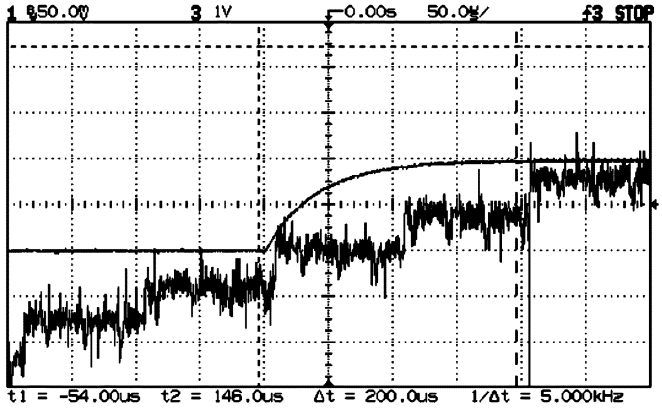

Fig. 11. Zero crossings of the input waveform and $v_{s\alpha}$.

The waveform $v_{s\alpha}$ reaches zero just one sampling time after the ideal zero crossing of the input signal, and it remains in zero during a whole sampling time, so $v_{s\alpha}$ rises from zero at the end of the second sampling interval after the ideal zero crossing of the input. This maximum delay in this example is at most 200 μs, or approximately 1% of the fundamental period of the input waveform. This delay can be reduced by increasing the sampling rate.

VI. Conclusion

This paper presented a simple method able to generate the sinusoidal reference waveforms used in certain control approaches for parallel active power filter applications or any other where such synchronization would be necessary (e.g., ac/dc converters for renewable energy resources, power factor correctors, power supplies, UPS, etc.). The method avoided the use of the conventional PLL and look up table configurations, by replacing them with a simple three-state dynamical system (when its most simple version is used) that provided the desired sinusoidal reference signals for controllers working in either the $\alpha\beta$ reference frame or the abc frame. The algorithm provides an output signal whose amplitude follows precisely the amplitude of the fundamental component of the input signal. Additionally, the method estimated the line fundamental frequency of the input signal within a bounded neighborhood of the actual value. One of the sinusoidal signals provided by the system is in phase (neglecting the delay of at most two sampling times that the simpler discrete realization introduces) with the fundamental frequency component of the input voltage, so no phase errors are introduced by false zero crossings of the input produced by noise or harmonics components. Note that standard PLL (e.g., [8]) use the zero crossing of the input as synchronizing signal, and that does not necessarily represent the zero crossing of the fundamental component of the input signal. Simulation and experimental results illustrated the high performance of the proposed method. Other possible applications of the method are the following: 1) to obtain an accurate estimation of the line frequency of a distribution system when synchronizing an isolated generator; 2) to replace the standard bandpass filters used in active filtering applications since the proposed system is not affected by the phase and amplitude

errors present in those filters under frequency variations when designed for sharp cutoff frequencies; and 3) to implement notch filters used in unbalance rejection algorithms for active magnetic bearings.

REFERENCES

[1] J. S. Tepper, J. W. Dixon, G. Venegas, and L. Morán, "A simple frequency-independent method for calculating the reactive and harmonic current in a nonlinear load," *IEEE Trans. Ind. Electron.*, vol. 43, no. 6, pp. 647–658, Dec. 1996.

[2] T. Núñez-Zúñiga and J. Pomilio, "Shunt active power filter synthesizing resistive loads," *IEEE Trans. Power Electron.*, vol. 1, no. 2, pp. 273–278, Mar. 2002.

[3] S. Bhattacharya and D. Divan, "Design and implementation of a hybrid series active filter system," in *Proc. IEEE 26th Annu. Power Electronics Specialists Conf. (PESC'95)*, Jun. 1995, vol. 1, pp. 18–22, 189–195.

[4] S. Bhattacharya, D. Divan, and B. Benerjee, "Active filter solutions for utility interface," in *Proc. IEEE Int. Symp. Industrial Electronics (ISIE'95)*, Jul. 10–14, 1995, vol. 1, pp. 53–63.

[5] S. Bhattacharya, P.- T. Cheng, and D. M. Divan, "Hybrid solutions for improving passive filter performance in high power applications," *IEEE Trans. Ind. Appl.*, vol. 33, no. 3, pp. 732–747, May/Jun. 1997.

[6] K. Sozañski, R. Strzelecki, and A. Kempski, "Digital control circuit for active power filter with modified instantaneous reactive power control algorithm," in *Proc. IEEE 33rd Annu. Power Electronics Specialists Conf. (PESC'02)*, Jun. 23–27, 2002, vol. 2, pp. 1031–1036.

[7] S.-J. Huang and J.-Ch. Wu, "A control algorithm for three-phase three-wired active power filters under nonideal mains voltages," *IEEE Trans. Power Electron.*, vol. 14, no. 4, pp. 753–760, Jul. 1999.

[8] K. Chatterjee, B. Fernandes, and K. Dubey, "An instantaneous reactive volt-ampere compensator and harmonic suppressor system," *IEEE Trans. Power Electron.*, vol. 14, no. 2, pp. 381–392, Mar. 1999.

[9] J. Dixon, J. J. García, and L. Morán, "Control system for three- phase active power filter which simultaneously compensates power factor and unbalanced loads," *IEEE Trans. Ind. Electron.*, vol. 42, no. 6, pp. 636–641, Dec. 1995.

[10] P. Rodriguez, J. Pou, J. Bergas, J. I. Candela, R. P. Burgos, and D. Boroyevich, "Decoupled double synchronous reference frame PLL for power converters control," *IEEE Trans. Power Electron.*, vol. 22, no. 2, pp. 584–592, Mar. 2007.

[11] C. A. Busada, H. G. Chiacchiarini, and J. C. Balda, "Sinusoidal waveform synthesis for parallel active power filter applications," in *Proc. IEEE 35th Annu. Power Electronics Specialists Conf. (PESC'04)*, Jun. 20–25, 2004, vol. 3, pp. 2360–2364.

[12] M. Vidyasagar, *Nonlinear System Analysis*, 2nd ed. Upper Saddle River, NJ: Prentice-Hall, 1993.

[13] R. Herzog, B. Philipp, G. Conrad, and L. Rene, "Unbalance compensation using generalized notch filters in the multivariable feedback of magnetic bearings," *IEEE Trans. Control Syst. Technol.*, vol. 4, no. 5, pp. 580–586, Sept. 1996.

[14] L. O. Chua and P. Y. Lin, *Computer-Aided Analysis of Electronic Circuits: Algorithms and Computational Techniques*. Upper Saddle River, NJ: Prentice-Hall, 1975.

Claudio Alberto Busada was born in Bahía Blanca, Argentina, on March 13, 1962. He received the B. Sc. degree in electrical engineering in 1989 and the Ph.D. degree in control systems in 2004, both from the Universidad Nacional del Sur, Bahía Blanca.

From 1988 to 2004, he was with the Mechanic and Electrical Department, City of Bahía Blanca. Since 1989, he has been with the Departamento de Ingeniería Eléctrica y de Computadoras (DIEC), Universidad Nacional del Sur, where he is a Professor. He is also a Researcher with the Instituto de Investigaciones en Ingeniería Eléctrica "Alfredo C. Desages" (UNS-CONICET). His areas of research include power electronics, rotating machinery, active filters, automatic control, and electric vehicle propulsion.

Héctor Gerardo Chiacchiarini (M'88–SM'04) was born in Villa Regina, Argentina, in 1964. He received the B.Sc. degree in electronics engineering from the Universidad Nacional del Sur, Bahía Blanca, Argentina, in 1990. He was granted a scholarship from CONICET during 1990–1997 for his posgraduate studies. and received the Ph.D. degree in control systems in 1996, also from the Universidad Nacional del Sur.

He is a Professor at the Departamento de Ingeniería Eléctrica y de Computadoras, Universidad Nacional del Sur, teaching power electronics and industrial robotics. He has been a Researcher since 1999 at the Instituto de Investigaciones en Ingeniería Eléctrica "Alfredo C. Desages" (UNS-CONICET). His main research interests are power electronics, robotics, mechatronics, motor drives, and control systems.

Dr. Chiacchiarini is a member of the Industrial Electronics Society. He was President of the Joint Chapter (RAS, CSS, IAS, IES, PELS) of the IEEE Argentina Section during 2005–2006 and Vice President during 2003–2004.

Juan Carlos Balda (M'78–SM'94) was born in Bahía Blanca, Argentina. He received the B.Sc. degree in electrical engineering from the Universidad Nacional del Sur, Bahía Blanca, Argentina, in 1979 and the Ph.D. degree in electrical engineering from the University of Natal, Durban, South Africa, in 1986.

He was with Hidronor S.A., an electric utility in the Southwestern part of Argentina, prior to his graduate studies. He was later a Researcher and a part-time Lecturer at the University of Natal until July 1987. He then spent two years as a Visiting Assistant Professor at Clemson University, South Carolina. He has been at the University of Arkansas at Fayetteville since July 1989, where he is currently a Full Professor and Associate Department Head, and Faculty Advisor to the Ham Radio Club at the University of Arkansas. His main research interests are power electronics, electric power distribution systems, motor drives and electric power quality.

Dr. Balda is a member of the Power Electronics and Industry Applications Societies of the IEEE and the honor society Eta Kappa Nu. He is a counselor of the IEEE Student Branch